Earth Syst. Dynam., 15, 91–108, 2024
https://doi.org/10.5194/esd-15-91-2024

Earth System Dynamics
Open Access
EGU

Future water storage changes over the Mediterranean, Middle East, and North Africa in response to global warming and stratospheric aerosol intervention

Abolfazl Rezaei[1,2], Khalil Karami[3], Simone Tilmes[4], and John C. Moore[5]

[1]Department of Earth Sciences, Institute for Advanced Studies in Basic Sciences (IASBS), Zanjan 45137-66731, Iran
[2]Center for Research in Climate Change and Global Warming (CRCC), Institute for Advanced Studies in Basic Sciences (IASBS), Zanjan 45137-66731, Iran
[3]Institut für Meteorologie, Stephanstraße 3, 04103 Leipzig, Germany
[4]National Center for Atmospheric Research, Boulder, CO, USA
[5]Arctic Centre, University of Lapland, Rovaniemi, 96101, Finland

Correspondence: Abolfazl Rezaei (arezaei@iasbs.ac.ir, abolfazlrezaei64@gmail.com)

Received: 20 July 2023 – Discussion started: 31 July 2023
Revised: 24 October 2023 – Accepted: 3 November 2023 – Published: 29 January 2024

Abstract. Water storage plays a profound role in the lives of people across the Middle East and North Africa (MENA) as it is the most water-stressed region worldwide. The lands around the Caspian and Mediterranean seas are simulated to be very sensitive to future climate warming. Available water capacity depends on hydroclimate variables such as temperature and precipitation that will depend on socioeconomic pathways and changes in climate. This work explores changes in both the mean and extreme terrestrial water storage (TWS) under an unmitigated greenhouse gas (GHG) scenario (SSP5-8.5) and stratospheric aerosol intervention (SAI) designed to offset GHG-induced warming above 1.5 °C and compares both with historical period simulations. Both mean TWS and extreme TWS are projected to significantly decrease under SSP5-8.5 over the domain, except for the Arabian Peninsula, particularly in the wetter lands around the Caspian and Mediterranean seas. Relative to global warming, SAI partially ameliorates the decreased mean TWS in the wet regions, while it has no significant effect on the increased TWS in drier lands. In the entire domain studied, the mean TWS is larger under SAI than pure GHG forcing, mainly due to the significant cooling and, in turn, a substantial decrease in evapotranspiration under SAI relative to SSP5-8.5. Changes in extreme water storage excursions under global warming are reduced by SAI. Extreme TWS under both future climate scenarios is larger than throughout the historical period across Iran, Iraq, and the Arabian Peninsula, but the response of the more continental eastern North Africa hyper-arid climate is different from the neighboring dry lands. In the latter case, we note a reduction in the mean TWS trend under both GHG and SAI scenarios, with extreme TWS values also showing a decline compared to historical conditions.

1 Introduction

The Middle East and North Africa (MENA), with 6 % of the world's population, are currently among the most water-stressed regions worldwide (Fragaszy et al., 2020). The dry climate, intensifying droughts, increasing population, and water over-extraction, particularly across the Middle East (World Bank, 2018), make it home to 12 of the 17 most water-stressed countries on the planet (Hofste et al., 2019). Water availability is crucial for sanitation (Reiter et al., 2004), economic activity (UNESCO, 2003), ecosystems (Shiklomanov and Rodda, 2003), and hydrological systems (Mooney et al., 2005).

The MENA region has the largest expected economic losses from climate-related water scarcity, robustly estimated at 6 %–14 % of gross domestic product (GDP) by 2050 (World Bank, 2018). MENA's terrestrial water storage (TWS) is being intensively extracted and may act as a flash point for conflict (Famiglietti, 2014). TWS incorporates all water on the land surface (snow, ice, water stored in the vegetation, rivers, and lake water) and in the subsurface (soil moisture and groundwater). Beyond anthropogenic activities, natural climate variability such as drought frequency affects water storage and agriculture, which then impacts food security (Fragaszy et al., 2020). The Middle East is especially prone to severe and sustained droughts due to its location in the descending limb of the Hadley circulation and associated dry and semiarid climate (Barlow et al., 2016). The 1998–2012 14-year period was the worst drought in the past 900 years (Cook et al., 2016). Because the saturated vapor pressure of air is largely controlled by temperature, any change in temperature, as well as precipitation, substantially affects (Konapala et al., 2020; Ajjur and Al-Ghamdi, 2021; Hobeichi et al., 2022) the water storage capacity available to supply the increasing water demand in the region (Lian, 2021). The MENA region, having both low precipitation and high evaporation, is very vulnerable to climate change (Giorgi, 2006; Lelieveld et al., 2012; Tabari and Willems, 2018; Zittis et al., 2019). MENA water storage is therefore particularly sensitive to any perturbation of the water cycle imposed by global warming.

GHG warming has already adversely affected water resources in the MENA region (Wang et al., 2018) and is simulated to intensify water competition between states (Arnell, 1999) in the future. Although global warming is expected to increase precipitation and soil moisture across MENA (Cook et al., 2020), it will decrease runoff and groundwater recharge by larger amounts (Milly et al., 2005; Shaban, 2008; Suppan et al., 2008). Using the GHG emission scenario A1B simulated by nine CMIP3-class climate models, Droogers et al. (2012) projected that 22 % of the future annual water shortage, 199 km^3 in 2050 in MENA, will be due to global warming. A total of 17 global climate models from Coupled Model Intercomparison Project Phase 6 (CMIP6) under SSP5-8.5 simulate a significant increase in precipitation ($+0.05$ to 0.3 ± 0.1 mm d^{-1}) over the southeastern Sahara in North Africa (NA) by the end of the century (Arjdal et al., 2023). They also projected that the total soil moisture would increase over southern Sahara under the SSP5-8.5 (6 % to 20 %) and SSP2-4.5 (4 % to 14 %). Based on TWS data from eight global climate models participating in CMIP6, a broad part of the dry MENA region tends to be wetter under SSP5-8.5 over 2071–2100 (Xiong et al., 2022). GHG-driven groundwater storage depletion in the Middle East during the 21st century will far exceed that during the 20th century due to the increased evapotranspiration (ET) and reduced volume of snowmelt (Wu et al., 2020).

Although MENA's adjacent densely populated region, the Mediterranean, has a better water storage state, it is projected to substantially suffer from reduced water availability under future GHG climate scenarios (Lionello et al., 2006). This is due to both projected significant decreases in rainfall (MedECC, 2020) and large increases in demand for irrigation water by the end of the 21st century (Fader et al., 2016). The precipitation and water availability in the Mediterranean region, to the northwest of the MENA, is also projected to be highly sensitive to global warming, particularly regarding water availability (Lionello et al., 2006), having the largest differences in the water availability between 1.5 and 2 °C warming scenarios globally (Schleussner et al., 2016). Global warming decreases Mediterranean groundwater recharge according to simulations under the IPCC A2 and B2 scenarios simulated using ECHAM4 and HadCM3 models (Döll and Flörke, 2005). Runoff is decreased by 10 %–30 % according to 12 models such as CCSM3 and ECHAM5/MPI-OM (Milly et al., 2005), and soil moisture z scores (obtained by taking the difference from the average and then dividing it by the standard deviation of the time series from the baseline period) are decreased by -1 to -4 in warm seasons according to simulations under SSP1-2.6, SSP2-4.5, SSP3-7.0, and SSP5-8.5 (Cook et al., 2020). Water availability in turn is lowered by 8 %–28 % for a warming of 2 °C as simulated by 11 CMIP5-class models by Schleussner et al. (2016). Likewise, Döll et al. (2018) found a strong drying in the Mediterranean region under global warming since the largest precipitation decreases worldwide were simulated in this region under SSP1-2.6, SSP2-4.5, SSP3-7.0, and SSP5-8.5 scenarios (Cook et al., 2020). CMIP5 model results also confirm that global warming (RCP2.6 and RCP6.0) substantially decreases the TWS in the Mediterranean by the middle (2030–2059) to late (2070–2099) 21st century (Pokhrel et al., 2021).

If global mean surface temperature rises to exceed 1.5 °C above the pre-industrial mean temperature, severe global consequences and societal problems can be expected (Masson-Delmotte, 2022). Solar radiation modification (SRM), a form of intervention to cool the climate by reflecting sunlight, has been proposed as a potential method of limiting global temperature rises and the associated impacts of increased GHG emissions. SRM may be the only way to keep or reduce surface temperatures to 1.5 °C given the reality of the GHG mitigation measures that have been agreed upon to date (MacMartin et al., 2022). Simulations have shown that a 2 % decrease in total solar irradiance roughly offsets global warming due to a doubling of CO_2 concentrations, and continuous injections of 10–18 Tg SO_2 per year would lead to a cooling of about 1 °C after several years (WMO, 2022). This is consistent with observed surface cooling after large volcanic eruptions, such as the 1991 Mt. Pinatubo eruption, which produced cooling of about 0.3 °C over a 2–3-year period (e.g., IPCC, 2021).

Many global climate models have simulated SRM in the form of stratospheric aerosol intervention (SAI). Model studies include the Stratospheric Aerosol Geoengineering Large Ensemble Project GLENS (e.g., Cheng et al., 2019; Simpson et al., 2019; Abiodun et al., 2021), the Geoengineering Model Intercomparison Project (Kravitz et al., 2013; Tilmes et al., 2013), and others (e.g., Bala et al., 2008; Jones et al., 2018; Muthyala et al., 2018). Compared with global warming, SAI decreases mean global precipitation (Govindasamy and Caldeira, 2000; Bala et al., 2008; Robock et al., 2008; Cheng et al., 2019; Simpson et al., 2019) as well as both the intensity and frequency of precipitation extremes caused by GHG-induced climate change (Tilmes et al., 2013; Muthyala et al., 2018). The study by Dagon and Schrag (2016) is a rare article that focuses on the spatial variability of runoff and soil moisture responses to SRM. Although solar geoengineering weakens the global hydrologic cycle (e.g., Bala et al., 2008; Tilmes et al., 2013; Ricke et al., 2023), its regional impacts are method- and strategy-dependent (Ricke et al., 2023) with potentially substantial changes in the regional precipitation patterns (Ricke et al., 2010; Tilmes et al., 2013, 2020; Crook et al., 2015; Dagon and Schrag, 2016). While differences in temperature fields vary relatively smoothly with radiative forcing, precipitation patterns are far more variable, being dependent on atmosphere–ocean–land surface coupling on a wide range of spatial and temporal scales. Furthermore, SAI simulations rely on many model-specific details and parameterizations that tend to produce larger across-model differences than simulations using simpler forms of SRM (Visioni et al., 2021). While SAI may counteract the annual mean water availability changes over land forced by GHG, it is not easy to offset the regional consequences, especially in the hydrological cycle, such as the Amazonian drying trend and its reduced precipitation, evaporation, and precipitation minus evaporation (Jones et al., 2018).

Although the MENA region and the adjacent Mediterranean region are known to be a "hot spot" for climatic change (Giorgi and Lionello, 2008; Bucchignani et al., 2018), little has been done regarding potential changes in TWS across MENA, especially under SRM climates. This study fills that knowledge gap and explores the changes that may occur in TWS under (i) a high-GHG-emissions scenario and (ii) the same GHG scenario combined with SAI designed to globally neutralize the GHG radiative forcing, and it (iii) compares both future climates with historical conditions (1985–2014) across the Mediterranean, Middle East, and NA.

2 Data and methods

2.1 Study area

The study area is composed of MENA and southern Europe to its north including the Caspian and Mediterranean seas. MENA covers the large region from Morocco in the west to Iran in the east, containing all the Maghreb and the Middle Eastern countries from 15 to 45° N latitude and from 20° W to 63° E longitude (Fig. 1). As well as being a water-stressed region, MENA is a worldwide hot spot for exacerbated extreme temperatures, aridity conditions, and drought (Giorgi and Lionello, 2008; Bucchignani et al., 2018). According to the Köppen climate classification system (Peel et al., 2007), MENA broadly has a hot and arid climate except for the coastal regions and highlands. Most of NA has a desert climate and 90 % is covered by the Sahara. The 2 m air temperature rises to 50 °C in summertime, while the annual mean precipitation is less than 25 mm (Faour et al., 2016). The arid steppe climate predominates in Morocco, Algeria, and Tunisia with cold winters (Faour et al., 2016) except for the Atlas Mountains, which are cooler and wetter (annual mean precipitation of $\sim$ 500 mm).

Across the Middle East, the largest amount of precipitation falls in four main regions: the coastal eastern Mediterranean Sea, the southern coast of the Caspian Sea, the western sides of the Zagros Mountains across Iran and Iraq, and the southern tip of the Arabian Peninsula. The Middle East also contains several major deserts having little to no precipitation: the Lut and Kavir deserts in the southeastern and north–central regions in Iran, the Arabian Desert, the Syrian Desert, and the Negev in the southeastern corner of the Mediterranean Sea. Middle East precipitation often originates from moisture coming from the west over the Mediterranean Sea (Evans and Smith, 2006). The Red Sea and the Persian Gulf are also source regions for the heaviest precipitations across the area.

The Mediterranean area has mild wet winters and warm to hot dry summers, as well as a complicated morphology, owing to the many steep orogenic structures and distinct basins and gulfs, along with islands and peninsulas of various sizes (Lionello et al., 2006).

Based on its full range of climate types, we divided the study area into six subregions (R1 to R6) to explore the changes in hydroclimate variables under both global warming and SAI scenarios (Fig. 1). The regions R1 to R6 respectively refer to the lands around the Caspian Sea, eastern Middle East (largely containing Iran and Iraq), Mediterranean area, Arabian Peninsula, eastern NA, and western NA. The simulated present-day climatology (1985–2014) of each region for different hydrological quantities is summarized in Table 1. Potential evapotranspiration (ET) is the amount of evaporation that would occur if a sufficient water source were available. The Thornthwaite method was used to calculate the potential ET based on the monthly mean temperature and latitude data for each grid. Evaporation from both soil and canopy and transpiration are summed up to obtain the real ET, which is the quantity of water actually removed from a surface by evaporation and transpiration. The lands around the Caspian and Mediterranean seas with a cooler climate have the highest precipitation and real ET, while more continental eastern NA with hyper-arid climate (with annual pre-

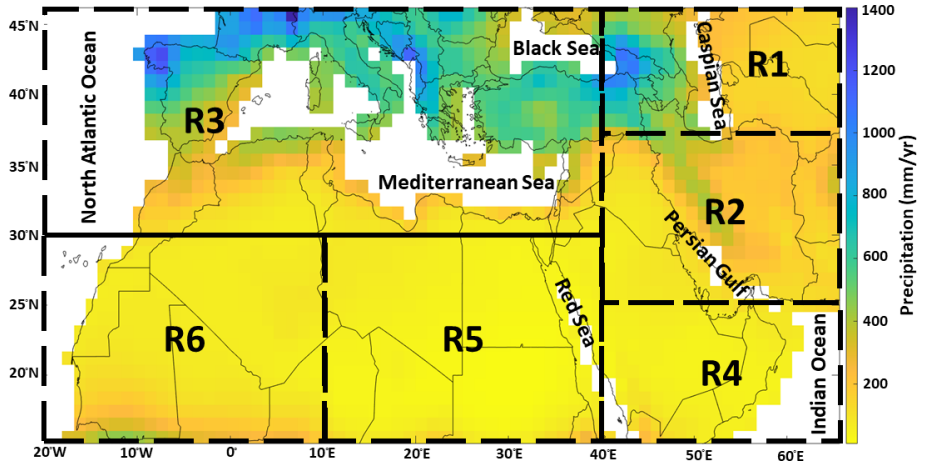

Figure 1. MENA annual precipitation map during the historical period. Regions R1 to R6 largely refer to the lands around the Caspian Sea, the eastern Middle East (largely containing Iran and Iraq), the Mediterranean area, Arabian Peninsula, eastern North Africa (NA), and western NA, respectively.

cipitation less than 100 mm) has the lowest precipitation, real ET, soil moisture, and TWS. The lands around the Caspian Sea have the highest soil moisture and TWS. More continental refers to an area with characteristics that are typical of continental climates and is less influenced by the moderating effects of nearby oceans.

2.2 Model simulations and scenarios

We examined the data from the NCAR Community Earth System Model version 2–Whole Atmosphere Community Climate Model Version 6 (CESM2(WACCM6)) that simulated the CMIP6 (Eyring et al., 2016) scenarios. CESM2 ranks among the top nine models known for their accuracy in simulating global precipitation patterns based on the Hellinger distance metric, which compares the bivariate empirical densities of CESM2 with those of 34 CMIP6 models against historical precipitation data sourced from the Global Precipitation Climatology Centre (GPCC) (Abdelmoaty et al., 2021). CESM2 has precipitation biases about 20 % lower than CESM1 (Danabasoglu et al., 2020). CESM2(WACCM6) has an interactive stratospheric aerosol treatment (Danabasoglu et al., 2020) that is consistent with observations (Mills et al., 2016). For global terrestrial ET, CESM2(WACCM6) ranked as the second-best model among 19 CMIP6 models (Wang et al., 2021). Furthermore, CESM2(WACCM6) reproduced the observed global land carbon trends remarkably well (Danabasoglu et al., 2020) and includes a full ocean model (Parallel Ocean Program version 2, POP2) to simulate the response of stratospheric aerosol change in the climate.

CESM2 also demonstrates satisfactory performance in simulating historical climate conditions within the study area. In the evaluation by Babaousmail et al. (2021), which assessed 15 CMIP6 models in replicating monthly rainfall patterns spanning 1951 to 2014 in NA, CESM2(WACCM6) emerged as one of the top-performing models. It accurately captured rainfall peaks across the region, albeit with a slight overestimation (ranging from 5 to 10 mm month^{-1}) in the southern areas and a slight underestimation (ranging from 0 to 20 mm month^{-1}) in the northern regions. Despite these minor deviations, CESM2(WACCM6) was recognized as one of the models that can simulate precipitation patterns well across NA, achieving a Taylor skill score of 0.62. Evaluation of CESM2(WACCM6) across the Mediterranean coasts placed it at the 9th and 17th positions out of 31 CMIP6 models for its performance in simulating temperature and precipitation (Bağçaci et al., 2021). Furthermore, when it comes to simulating precipitation relative to observational data for northeastern Iran during the period of 1987–2005, CESM2 stood out as the top-performing model among six CMIP6 models (Zamani et al., 2020). Assessing the representation of spatial and temporal variations in historical precipitation from 1980 to 2014 across Africa and the Arabian Peninsula, the CMIP6 multi-mean ensemble (inclusive of CESM2(WACCM6)) demonstrated reasonable performance, as highlighted in Nooni et al. (2023).

The SAI simulation we use (SSP5-8.5-SAI) is designed to employ SAI together with the high-GHG-emissions scenario, SSP5-8.5, with the target of limiting mean global temperatures to 1.5 °C above pre-industrial (1850–1900) conditions (Tilmes et al., 2020). Under SSP5-8.5 forcing, Tilmes et al. (2020) projected that this threshold is exceeded around the year 2020 in CESM2(WACCM6). The atmospheric component of CESM2(WACCM6) has a resolution of 1.25° in longitude and 0.9° in latitude. The experiment injects SO_2 at 180° longitude at four predefined latitudes (30° N, 30° S, 15° N, and 15° S) at around 25 km at 15° N/S and around 22 km at 30° N/S as suggested by Tilmes et al. (2018) using a feedback control algorithm to maintain not just the

Table 1. The medians of precipitation, temperature, real evapotranspiration (ET), soil moisture, terrestrial water storage (TWS), and potential ET over each region (R1 to R6, see Fig. 1) during the historical period according to the model outputs. The results for global warming and SAI are further shown in Table S1.

Region	R1	R2	R3	R4	R5	R6
Precipitation ($mm\,yr^{-1}$)	321	182	479	78	48	112
Temperature (°C)	14.2	20.5	17.2	27.0	23.7	25.3
Real ET ($mm\,yr^{-1}$)	419	187	388	72	50	112
Soil moisture ($kg\,m^{-2}$)	1846	1771	1572	1353	1155	1287
TWS ($kg\,m^{-2}$)	2091	1776	1623	1358	1167	1313
Potential ET ($mm\,month^{-1}$)	74	123	74	210	143	185

global mean temperature, but also the interhemispheric and Equator-to-pole temperature gradients (Tilmes et al., 2020). For SSP5-8.5-SAI, most of the sulfur mass was injected at 15° S, with some at 15° N and 30° S and very little at 30° N. We used the monthly TWS (the sum of snow water equivalent and soil moisture; Wu et al., 2021), precipitation, temperature, water evaporation from soil and canopy, transpiration, soil moisture, and leaf area index (LAI) data from all five ensemble members (r1 to r5) of the SSP5-8.5 scenario and the three available ensemble members (1–3) of SSP5-8.5-SAI. The results for variables other than TWS are shown in the Supplement. For the historical period, we used all three available realizations (r1 to r3) from CESM2(WACCM6). For the anomaly analysis relative to historical conditions and the multiple linear regression models, we used the first three ensembles of SSP5-8.5, consistent with the three available historical members. We compare the GHG and SAI scenarios over 2071–2100 with the 1985–2014 historical period.

We focused on the historical period from 1985 to 2014 rather than the entire historical dataset spanning from 1850 to 2100 for several reasons. Firstly, recent historical climate data may exhibit less uncertainty, given that additional meteorological stations with improved data quality are available to be used for model calibrations (Zhang et al., 2020). Secondly, this selected historical period offers valuable insights into the observable impacts of climate change, which are highly pertinent to present-day societal and environmental challenges. These insights are of utmost importance to policymakers and communities alike. Thirdly, the chosen historical 30-year time period aligns with the 30-year periods considered for the GHG emissions and SAI scenarios, ensuring consistency in our statistical analysis. We focus on the 2071–2100 future period because the anticipated changes in TWS driven by GHG emissions are expected to be more pronounced during this time frame (Pokhrel et al., 2021). Furthermore, the SAI forcing is strongest in the later period of the simulation and is expected to produce a more significant result.

2.3 Return periods

We are interested in climate extremes, not only changes in means. Therefore, we examine how the frequency of events of some particular levels is likely to change under different scenarios. We use the generalized extreme value (GEV) distribution function to estimate the probability distribution function of the TWS extremes. A return period is an estimated average time between events such as floods or river discharge flows. It is calculated by generating the 95 % normal-approximate confidence intervals in accordance with the mean and variance of the variable (here TWS).

The GEV probability density and cumulative distribution functions are defined as (Gilleland, 2020)

$$g(z) = \frac{1}{\sigma} t(z)^{1+\xi} e^{-t(z)};$$
$$G(z) = e^{-t(z)};\ t(z) = \begin{cases} \left\{1+\xi\left(\frac{z-\mu}{\sigma}\right)\right\}^{-1/\xi}, & \xi \neq 0 \\ e^{-\left(\frac{z-\mu}{\sigma}\right)}, & \xi = 0. \end{cases} \quad (1)$$

For $\xi \neq 0$, we have $t(z)^{1+\xi} = \left\{1+\xi\left(\frac{z-\mu}{\sigma}\right)\right\}^{-(1+1/\xi)}$ and for $\xi = 0$, the z domain restricted to $\xi\left(\frac{z-\mu}{\sigma}\right) > -1$. The GEV distribution is parameterized using ξ, μ, and σ, which are the shape, location, and scale parameters, respectively, and analogous to the skewness, mean, and standard deviation. We assume that the GEV is the valid distribution function for variables $z_1, \ldots, z_n$ representing the annual maximum return TWS levels, where the quantiles of the distribution function give the return levels, z_p. The return levels are the solutions to $G(z_p) = 1 - p$, which yields (Gilleland, 2020)

$$z_p = \begin{cases} \mu - \frac{\sigma}{\xi}[1 - \{-\ln(1-p)\}^{-\xi}] & \text{for } \xi \neq 0 \\ \mu - \sigma \ln\{-\ln(1-p)\} & \text{for } \xi = 0, \end{cases} \quad (2)$$

where p is probability corresponding to z_p. The return period is obtained as

$$\text{return period}\,(i) = 1/(1 - \text{cdf}(i)), \quad (3)$$

where cdf is the cumulative distribution function. We also calculated the 95 % asymptotic lower and upper confidence intervals based on the Kolmogorov–Smirnov statistic (Doksum and Sievers, 1976). We used the concatenated TWS

anomaly data for the historical period, high-GHG-emissions, and SAI scenarios to analyze the return periods. As an example, the relationship between empirical quantiles and model quantiles as well as the probability density versus quantiles for regions R2 and R5 are shown in Figs. S1 and S2 in the Supplement.

2.4 Multiple linear regression (MLR) model

We want to analyze how the primary driving climate fields (surface air temperature, precipitation, ET, and LAI – i.e., vegetation coverage) for TWS vary spatially and among the different scenarios (Zhang et al., 2022). We use a simple multiple linear regression (MLR) model with TWS as the dependent variable (Y) for each ensemble member in each region. The following procedures were conducted.

i. The variable clustering (VARCLUS) procedure was employed to thoroughly assess collinearity among the variables. VARCLUS is a method that effectively segregates a set of numeric variables into disjoint or hierarchical clusters, each characterized by a linear combination of the variables within the cluster (Sarle, 1990). The criterion is that when the proportion of the variance explained by a cluster is larger than 0.8, it is advisable to select one variable from that cluster. Based on the results obtained from VARCLUS (Figs. S3 and S4), we made specific decisions to enhance the robustness of our analysis. For instance, we identified strong correlations exceeding 0.9 between potential ET and temperature (Tables S2–S13), as well as between soil moisture and TWS in all cases (except for the eastern NA (R5) in Tables S2–S13). Consequently, we chose to exclude potential ET and soil moisture from our analysis due to their high levels of correlation with temperature and TWS, respectively.

ii. A linear regression model was considered with potential independent variables (X): temperature, precipitation, real ET, and LAI. We conducted a temporal autocorrelation analysis on all these independent variables for each model. This analysis was carried out using the autocorrelation function at a 95 % confidence level. In all regions (except R4), the autocorrelation results indicated that the lags at the first and second months were statistically significant, while the third month lag was almost nonsignificant. Therefore, we modified the MLR model to include information from the 2 preceding months in these regions. However, in region R4, we observed different patterns. In this region, both real ET and temperature significantly depended on their respective conditions from the 2 previous months, while precipitation did not show this effect. Moreover, LAI in R4 exhibited dependencies on the first 3 and 4 preceding months under the SSP5-8.5 and SSP5-8.5-SAI scenarios, respectively. Consequently, we incorporated specific lagged months for each variable in R4.

iii. The outliers were identified using the Bonferroni p values (i.e., Bonferroni correlation) and then removed. Bonferroni correlation is a modification for p values when several dependent or independent statistical tests are being accomplished concurrently on a single dataset. A Bonferroni correction divides the critical p value by the number of comparisons being made (Bland and Altman, 1995). The number of outlier data points excluded varies from zero to 5 (over the 700 point) in the 36 models.

iv. The final model was fitted after removing the outliers. In all regions and scenarios, the MLR models are statistically significant at the 95 % level. The variance explained (R^2) varies from around 0.3 in the dry southern MENA to 0.89 and 0.96 in the wetter lands around the Caspian and Mediterranean seas.

v. The relative "importance" of the variables for TWS in the final model was assessed using the Lindeman, Merenda, and Gold (LMG) method (Lindeman et al., 1980), where the fractional variance accounted for is determined as the independent variable-order average over average contributions in models of different sizes. The LMG method considers the average contributions of each variable across different model sizes and then averages these averages to provide a more robust measure of variable importance. The LMG can be defined as (Grömping, 2007) follows.

$$\mathrm{LMG}(x_k) = \frac{1}{p!} \sum_{\text{Permutation}} \mathrm{seq}R^2(\{x_k\}\,|r) \tag{4}$$

where $\mathrm{seq}R^2(\{x_k\}\,|S_k(r)) = R^2(\{x_k\} \cup S_k(r)) - R^2(S_k(r))$ and $R^2(S) = \frac{\text{Model } SS(\text{model with regressors in set } S)}{\text{Total } SS}$. Orders have the same $S_k(r) = S$ summarize into a single summand, we therefore can re-write Eq. (4):

$$\mathrm{LMG}(x_k) = \frac{1}{p!} \sum_{S \subseteq \{x_1,\ldots,x_p\} \setminus \{x_k\}} n(S)\,!(p - n(S) - 1)!\mathrm{seq}R^2(\{x_k\}\,|S) \tag{5}$$

LMG has been recommended by Johnson and LeBreton (2004) and Grömping (2007) since it uses both direct effects and impacts adjusted for other regressors in the model. As the considered variables may be correlated with each other, when a new predictor is added to a model that already contains other predictors, its impact can be influenced by the presence of those other variables. The LMG method takes into account these interactions and adjusts the variable's contribution to reflect its unique impact while considering the

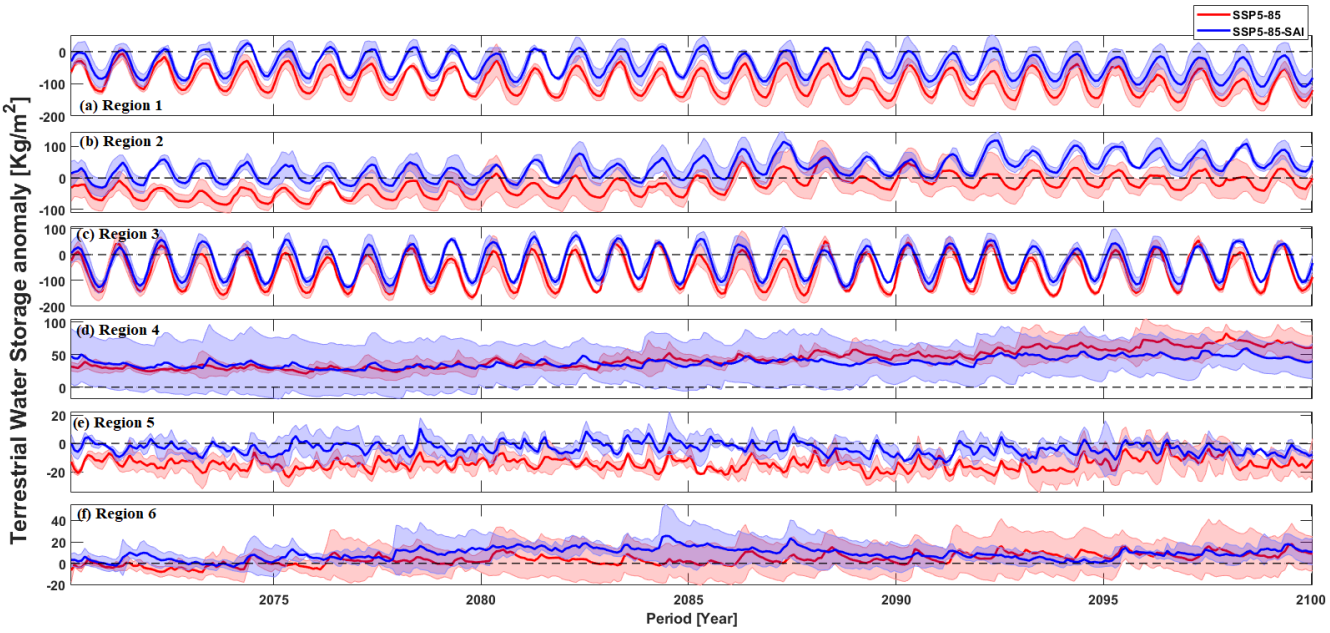

Figure 2. The TWS anomaly relative to the TWS averaged over the historical period across MENA and the lands around the Caspian and Mediterranean seas under global warming without (SSP5-8.5) and with SAI (SSP5-8.5-SAI). **(a–f)** Regions R1 to R6, respectively. Shading in each curve shows the across-ensemble range. The dashed line crossing the *y* axis at zero in each subplot is the ensemble mean of TWS over the historical period (1985–2014).

effects of other regressors. Importance is a unitless variable and the sum of all independent variable importance's in each model equals the model's explained variance. Here we use all three ensemble members separately to estimate the robustness of the importance estimates.

3 Results

3.1 Mean terrestrial water storage (TWS) changes due to GHG and SAI

In this section, we present the projected changes in TWS across MENA and the lands around the Caspian and Mediterranean seas. We discuss trends in the TWS anomalies relative to TWS averaged over the historical period (1985–2014) in response to both GHG (SSP5-8.5) forcing and to GHG + SAI. Figure 2 illustrates the original TWS anomalies, while Fig. S5 exclusively presents the long-term component, providing a clearer understanding of the changes under climate scenarios. The positive and negative anomalies in these figures refer to increasing and decreasing TWS, respectively. The trend decreases in the northern parts (R1 and R3) and eastern NA (R5) with a hyper-arid climate but rises in the Arabian Peninsula (R4) and western NA (R6) under both GHG and SAI scenarios, particularly over the latter part of the 21st century. In all regions, the SAI climate TWS is higher than SSP5-8.5 or at least lies in the across-range of SSP5-8.5 towards the end of the century, especially in R2 and R5 (Figs. 2 and S5). The TWS difference between SAI and global warming in region R2, particularly over the latter part of the 21st century, is greater relative to the rest of the domain. The TWS change is smaller in the hyper-arid eastern NA (R5) than the other regions under both climate scenarios.

Figure 3 depicts the TWS differences between the historical (1985–2014) and future climate scenarios over the 2071–2100 period. Consistent with the above findings, Figs. 3b and S6a–c show that the TWS response to GHG forcing in the wet regions around the Caspian (R1) and Mediterranean (R3) seas is simulated as declining, while across the (semi)arid MENA region, particularly in central Iran (R2), the Arabian Peninsula (R4), and the southern portions of NA (R5 and R6), there is a positive trend. Under global warming, the largest decrease in TWS occurs around the Caspian (particularly in the east) and the Mediterranean (except for its north), while its most robust increase happens in the southern margins of NA and the eastern parts of the Arabian Peninsula. SAI (Figs. 3c and S6d–f) partially counteracts the changes imposed by the increased GHG emission, particularly in the wetter lands around the Caspian and Mediterranean seas, which are simulated as experiencing TWS decrease under global warming. Temporal ensemble mean TWS due to GHG forcing (Fig. 3b) is only partially reversed by SAI (Fig. 3d), and the water storage shortfall is not fully canceled out by the intervention (Fig. 3c, d). However, simulated TWS in Iran and the southern half of MENA has greater water storage under SAI relative to the historical period (Fig. 3c).

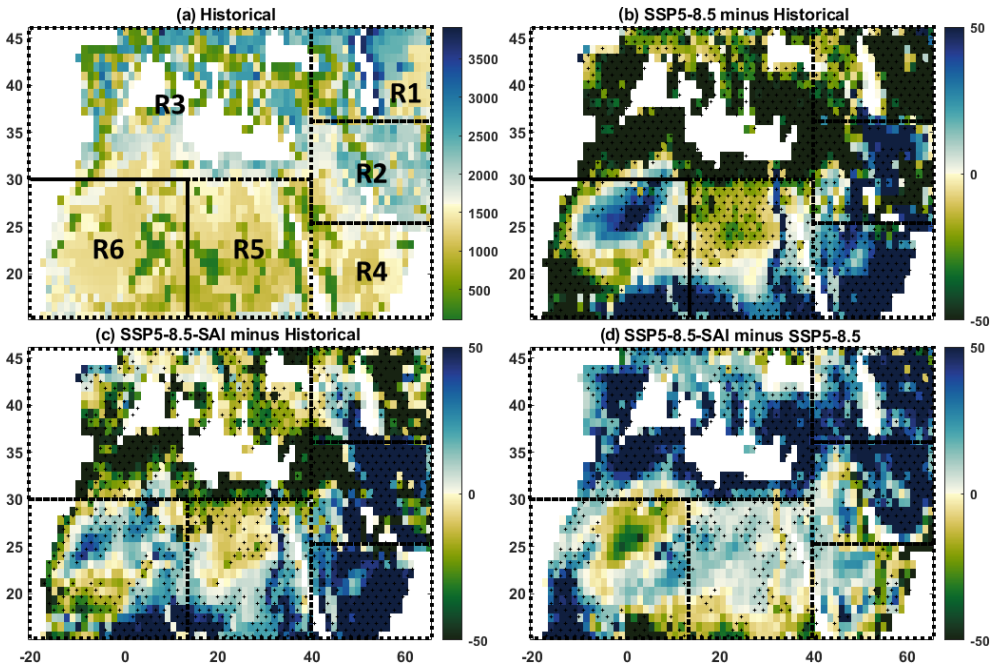

Figure 3. Ensemble mean maps of TWS (kg m^{-2}) across the studied domain in the historical climate **(a)** over 1985–2014 and their projected future changes in the 2071–2100 period under the SSP5-85 GHG scenario (SSP5-8.5 minus historical in panel **b** and GHG + SAI minus historical in **c**). The extent to which the SAI impacts the TWS changes imposed by global warming is further shown (SSP5-8.5-SAI minus SSP5-8.5 in **d**). Hatched areas show where all ensemble members agree on the sign of the changes.

In Fig. 4, we compare how simulated TWS statistical distributions vary between scenarios for each region. Mean TWS significantly ($p < 0.05$) decreases in the wetter lands around the Caspian (R1) and Mediterranean (R3) seas to the north (3.7 %–5.2 % on area average), while it significantly increases in the dry region of the Arabian Peninsula (5.6 %) in response to GHG warming. SAI, on the whole, partially reverses the projected changes in TWS from increasing GHG concentrations toward its historical values. Interestingly, SAI overcompensates for the TWS changes imposed by the high GHG forcing in Iran and Iraq (R2) where this region shows no significant change under GHG emissions (Fig. 4b). SAI also has an amplifying effect in R5 and a slight overcompensation in R6, but its impact is statistically insignificant.

We also compared the changes in TWS with changes in precipitation, temperature, real ET, soil moisture, and potential ET over each region under both global warming and SAI scenarios (Figs. S7 to S10). The TWS decreasing patterns under both SSP5-8.5 and SSP5-8.5-SAI scenarios across the entire study area are similar to soil moisture change patterns (Figs. S7 and S9) but are more widespread than precipitation under global warming (Fig. S9). Notably, in the Mediterranean and the dry MENA region, the soil moisture variability accounts for the dominant component of TWS variability (Pokhrel et al., 2021). However, decreased TWS is seen beyond the regions of reduced precipitation (Fig. S9), from beyond the Mediterranean and Atlantic coasts to include Syria, Iraq, and the lands around the Caspian Sea as well as to a wide portion of NA (Fig. 3). These include places where precipitation is either increasing or shows no significant change, consistent with results reported by Cook et al. (2020).

In summary, our findings show that the SSP5-8.5-SAI scenario has a potential to partially offset the significant changes in mean TWS imposed by SSP5-8.5 over the entire MENA. While SAI (Fig. 3d) succeeded in reversing mean TWS deficits in the wetter lands around the Caspian and Mediterranean seas driven by the GHG SSP5-8.5 scenario (Fig. 3b), it did not fully cancel out the TWS deficits (Figs. 3c, 4a, c). However, in the dry MENA regions (Fig. 3d), particularly Iran (containing the Lut desert in the southeastern region and the Kavir desert in the north–central region), Iraq, and the Arabian Peninsula (housing the Arabian Desert), SAI resulted in higher mean water storage relative to the historical period (Figs. 3c and 4).

3.2 Changes in extreme TWS

We compared changes in the expected return frequency of comparatively rare events to those during the historical period. Changes in mean conditions discussed so far are clear, but the changes in extremes display even larger separations between those expected under pure GHG forcing and the GHG + SAI scenarios. An increase in the return level or decrease in the return period of TWS means that the rare levels of high water availability increase, while a decrease in re-

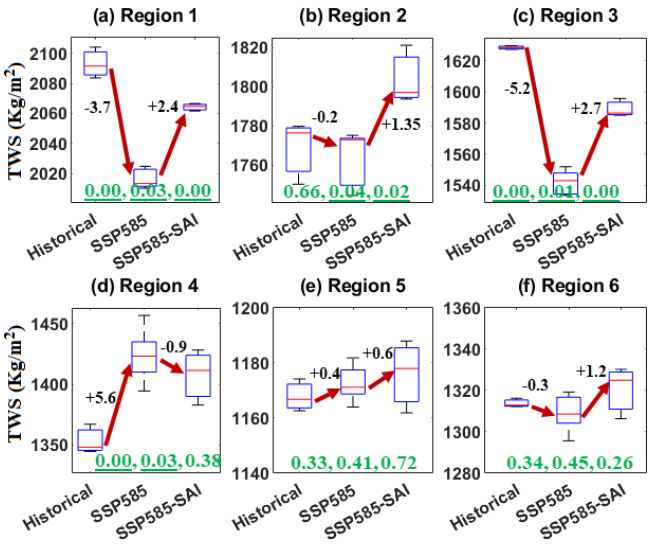

Figure 4. Box-and-whisker plot of the changes in terrestrial water storage (TWS) in regions 1 to 6 over 2071–2100 under SSP5-8.5 and SSP5-8.5-SAI relative to historical conditions (1985–2014). The titles of subplots refer to the regions. The median for each experiment is denoted by the red line, the upper (75th) and lower (25th) quartiles by the top and bottom of the box, and ensemble limits by the whisker extents. The positive and negative values in black are the change percent under SSP5-8.5 and SSP5-8.5-SAI relative to the median of the historical period data. The three values in green refer to p values between historical and global warming, historical and SAI, and global warming and SAI, obtained from a t-test analysis in which the underlined p values are statistically significant.

turn level for a given period means that rich water availability events become rarer. We applied a GEV distribution to the complete dataset of monthly TWS values without explicitly setting maximum values in Fig. 5. For comparison, we also extracted the annual maximum TWS values and provided the corresponding fitted GEV distribution. Overall, the probability densities for both datasets exhibit a high degree of similarity across various regions and scenarios (e.g., Figs. S11 and S12). Additionally, the graphs depicting return levels versus return periods based on annual maximums (Fig. S13) closely resemble the results obtained from the entire dataset (Fig. 5). In all cases, the trends are highly similar (compare Figs. 5 and S13), although it is worth noting that the annual maximum scenario exhibits slightly wider upper and lower bounds compared to the entire dataset scenario. We therefore focused on the results obtained from the entire dataset. Figure 5 shows the return levels versus return period curves with the 95 % lower and upper bands. To determine which curves (including its upper and lower bounds) are significantly different from each other (p values less than 0.05), we first conducted repeated-measure analysis of variance, which compares means across one or more variables that are based on repeated observations, and then performed post hoc Tukey–Kramer comparisons. The expected return levels versus return period curves (Fig. 5) decrease in response to both GHG warming and GHG + SAI in the Caspian and Mediterranean Sea areas (R1 and R3) as well as in the eastern NA (R5), as a more continental dry land, but increase in the Arabian Peninsula (R4) and western NA (R6). In Iran and Iraq (R2), SAI leads to a significant increase in expected TWS return levels relative to both historical conditions and the high-GHG-emission scenarios (Fig. 5b), while SAI tends to partially counteract the GHG-driven TWS changes in R1, R3, R4, and R5. Larger TWS levels are expected for the entire MENA compared with the GHG climate alone, particularly in Iran, Iraq, and western NA. Nonetheless, compared to the historical period, the Arabian Peninsula (Fig. 5d) is the region with the most robust increase in extreme TWS under both the global warming and SAI scenarios. Extreme TWS in the neighboring dry land of eastern NA with a hyper-arid climate is still smaller than the historical conditions.

Table 2 quantitatively compares the differences between TWS (and its corresponding 95 % lower and upper bounds in Fig. 5) changes at 30-, 50-, and 100-year return periods under historical, global warming, and SAI scenarios. Global warming, on the whole, decreases the TWS extremes (i.e., fewer wetter conditions) at 30- to 100-year return periods over all the study areas except for the Arabian Peninsula (R4) and western NA (R6). The most robust decreases in the extreme TWS imposed by global warming relative to historical conditions occurring in the lands around Caspian R1 (−108 % on average over return periods from 30 to 100 years), Mediterranean R3 (−43 % on average), and eastern NA R5 (−89 % on average) are partially suppressed by SAI. A small increase in extreme TWS in Iran and Iraq (R2) simulated under GHG (+15 %) is overcompensated for by SAI (+65 %). Although SAI decreases the TWS in the Arabian Peninsula (−11 %) relative to global warming, it still tends to experience the most robust extreme water storage increases in the future (+153 %) compared with historical conditions. In western NA (R6), the SAI simulation slightly intensifies the increased extreme TWS imposed by high GHG emissions by +27 %. Although SAI partially compensates for the changes over most of the study area (positive SSP5-8.5-SAI minus SSP5-8.5 values in Table 2), on the whole, extreme TWS tends to increase in the dry regions of Iran and Iraq, the Arabian Peninsula, and western NA while substantially decreasing in the wetter lands around the Caspian and Mediterranean seas, and to lower degrees, in the eastern NA as a more continental dry land compared with historical conditions.

3.3 Drivers of TWS change

To assess which variables have the most impact on mean TWS under both global warming and SAI, we fitted an MLR model to each ensemble member separately in each of the six regions (Figs. 6 and 7). The most important variable for the mean TWS under both global warming and SAI scenarios is region-specific. In the wet lands surrounding the Caspian

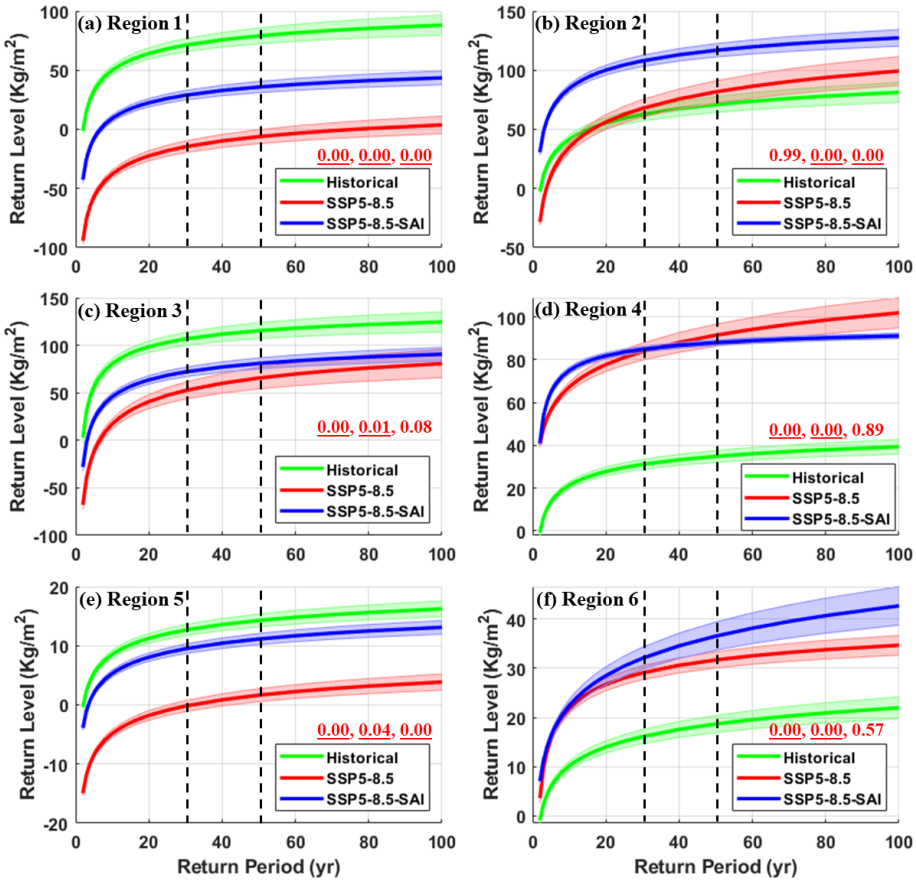

Figure 5. The TWS anomaly return level versus return period using the first three realizations for the historical, SSP5-8.5, and SSP5-8.5-SAI in regions 1 to 6 **(a–f)**. The two parallel dashed black lines refer to 30- **(a, c, e)** and 50-year **(b, d, f)** return periods. Shading in each curve represents the 95 % upper and lower confidence bands. The three values in red refer to p values between historical and global warming, historical and SAI, and global warming and SAI, obtained from repeated-measure analysis of variance and post hoc Tukey–Kramer comparisons in which the underlined p values are statistically significant.

(R1) and Mediterranean (R3) seas, temperature and precipitation are the primary drivers of TWS changes. In contrast, in the Middle East, characterized by predominantly dry climates (R2 and R4), vegetation coverage (i.e., LAI) plays a dominant role. This observation aligns with the fact that temperature limits ET in the wet regions, while in arid and hot regions, the availability of water for ET is the predominant limiting factor (Bao et al., 2021). In NA, where TWS changes are irregular (Fig. 2), temperature holds the greatest significance in the eastern regions (R5), while real ET is the primary driver in the west (R6). Warmer climate enhances the atmospheric water content over regions and seasons (Cook et al., 2020) since 1 °C warming is accompanied by ~ 7 % enhancement in the air water storage capacity (Trenberth, 2011) and, in turn, increases the evaporative demand (Arnell, 1999), and vice versa for cooler conditions. Real ET itself is mostly controlled by temperature and available water for evaporation (i.e., precipitation, soil moisture, and vegetation coverage). With just temperature and precipitation as independent variables, we find that the temperature under both global warming and SAI is generally more important for TWS than precipitation over the wet lands around the Caspian and Mediterranean seas as well as eastern NA. In contrast, precipitation plays a stronger role in TWS in Iran, Iraq, and western NA with lower precipitation under both future climate scenarios.

The regression models indicate that TWS is mostly driven by the combined impacts of changes in vegetation coverage, real ET, temperature, and precipitation, consistent with the fact that precipitation is not the only controlling factor for water resources (Cook et al., 2014; Wu et al., 2020). However, the temperature in the Mediterranean area with the highest precipitation over the entire domain studied plays a more important role than precipitation, vegetation coverage, and real ET under both warming and SAI scenarios.

Caution is required when interpreting the relative importance of results for the arid regions of R4 to R6 as their variance explained ($R^2 = 0.3$ to 0.52) from the MLR models is smaller than those (up to 0.89 and 0.96) for the wetter lands around the Caspian and Mediterranean seas. This, most prob-

Table 2. The percent differences (%) between the medians of the TWS return level at 30-, 50-, and 100-year return periods using the first three realizations for the historical, SSP5-8.5, and SSP5-8.5-SAI. Consistently, the value inside the parenthesis represents the percent difference range values between lower and upper 95 % confidence intervals from different scenarios.

	(SSP5-8.5 − historical)/historical · 100			(SSP5-8.5-SAI – historical)/historical · 100			(SSP5-8.5-SAI – SSP5-8.5)/historical · 100		
Region	30-year	50-year	100-year	30-year	50-year	100-year	30-year	50-year	100-year
R1	−121 (−130, −113)	−108 (−117, −100)	−96 (−105, −88)	−59 (−62, −57)	−55 (−57, −53)	−51 (−53, −49)	61 (56, 68)	53 (48, 60)	45 (40, 52)
R2	8 (6, 11)	15 (12, 17)	22 (20, 24)	73 (66, 81)	65 (58, 73)	57 (50, 65)	64 (55, 75)	50 (41, 60)	34 (25, 46)
R3	−51 (−56, −46)	−43 (−49, −38)	−35 (−42, −29)	−33 (−34, −32)	−30 (−31, −29)	−27 (−28, −26)	18 (14, 24)	13 (8, 20)	8 (2, 16)
R4	170 (163, 178)	163 (157, 169)	160 (155, 164)	173 (158, 191)	153 (138, 170)	132 (117, 150)	4 (−4, 13)	−10 (−19, 1)	−27 (−39, −14)
R5	−102 (−110, −95)	−89 (−96, −82)	−76 (−83, −70)	−25 (−26, −24)	−22 (−23, −21)	−19 (−20, −18)	77 (70, 84)	67 (61, 73)	57 (52, 63)
R6	80 (73, 89)	70 (63, 77)	58 (52, 65)	99 (95, 103)	95 (93, 99)	94 (93, 96)	18 (14, 22)	26 (21, 30)	36 (31, 41)

ably, arises from the arid to hyper-arid climate of R4 to R6 with small and irregular annual precipitation and, in turn, irregular TWS anomaly time series (Fig. 2d, e, f).

4 Discussion

We have analyzed the potential impacts of the unmitigated global warming SSP5-8.5 scenario (GHG) and the same GHG emissions trajectory with the addition of SAI (GHG + SAI) on both the mean and extreme water storage across the lands around the Caspian and Mediterranean seas, Middle East, and NA. We have used the CESM2(WACCM) climate model simulations with three realizations of each historical and SSP5-8.5-SAI scenario and five available realizations for SSP5-8.5. In response to high GHG emissions over the 2071–2100 period, the mean TWS decreases in the wetter regions (i.e., around the Caspian and Mediterranean seas with mild wet winters and warm to hot dry summers), in agreement with previous studies based on SSP5-8.5 (e.g., Cook et al., 2020; Scanlon et al., 2023), RCP2.6, and RCP4.5 (e.g., Döll et al., 2018), as well as with projections from 11 global hydrological models (Schewe et al., 2014) with globally forced 2 °C warming (Schleussner et al., 2016). Similarly, a decrease in precipitation (Kim and Byun, 2009), surface runoff (Cook et al., 2020), and TWS (Pokhrel et al., 2021) has been reported across Mediterranean coasts under GHG warming. In contrast, the mean TWS increases or shows no significant change in the MENA, housing several major deserts with minimal precipitation. The temporal ensemble mean TWS increase in the southern MENA is consistent with other climate model simulations showing increased precipitation and soil moisture in CMIP6 simulations under SSP5-8.5 (Cook et al., 2020) and SSP2-4.5 (Ajjur et al., 2021; Scanlon et al., 2023). This further aligns with a projected northward shift of the Intertropical Convergence Zone (ITCZ) in eastern Africa, mostly during the months of May to October (Mamalakis et al., 2020), leading to increased moisture transfer to the southern Middle East and NA (Waha et al., 2017).

Given the prevailing water scarcity challenges in many regions of the Middle East where population growth is a continuing concern (Oroud, 2008), by mitigating the vulnerability to global warming, SAI may offer a potential strategy to augment the regional water resources across the area, particularly in the dry regions of Iran (containing the Lut desert in the southeastern region and the Kavir desert in the north–central region), Iraq, and the Arabian Peninsula (housing the Arabian Desert), compared with the pure GHG-forced scenario. Similarity, Jones et al. (2018) found that SAI could effectively counteract the changes in available water imposed by global warming on Earth's lands. Mousavi et al. (2023) also found that increased soil moisture and enhanced vegetation coverage would lead to the reduction of dust concentration in the MEAN region under SAI.

The more robust and widespread deficit in mean TWS compared to precipitation in the area, which is in line with results reported by Cook et al. (2020), highlights the profound roles that other variables or processes have in the increased ET such as greater atmospheric moisture demand (Dai et al., 2013, 2018) and greater vegetation water use (Mankin et al., 2019) owing to warmer conditions under global warming, consistent with regression model results. According to MLR model results (Figs. 6 and 7), the projected changes in TWS were not solely attributable to precipitation; its inter-

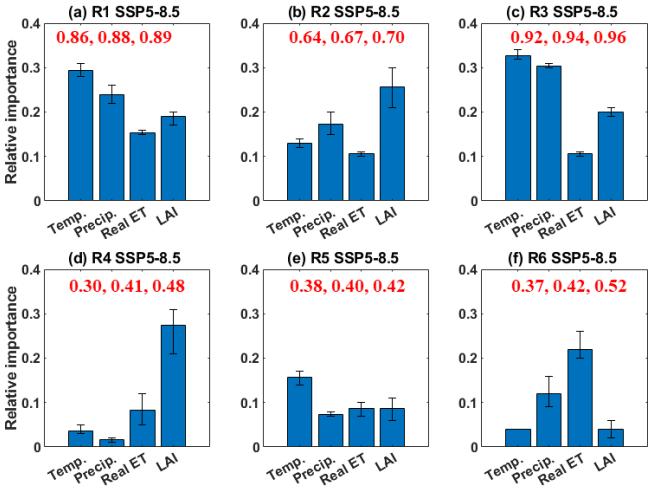

Figure 6. LMG importance plot (Lindeman et al., 1980) of the four independent variables in the regression for TWS for the global warming SSP5-8.5 scenario in each region. The bar and range bar respectively show the ensemble mean importance and the range of importance from the three ensemble members. The three values in red in each subplot show the minimum, mean, and maximum variances explained by models.

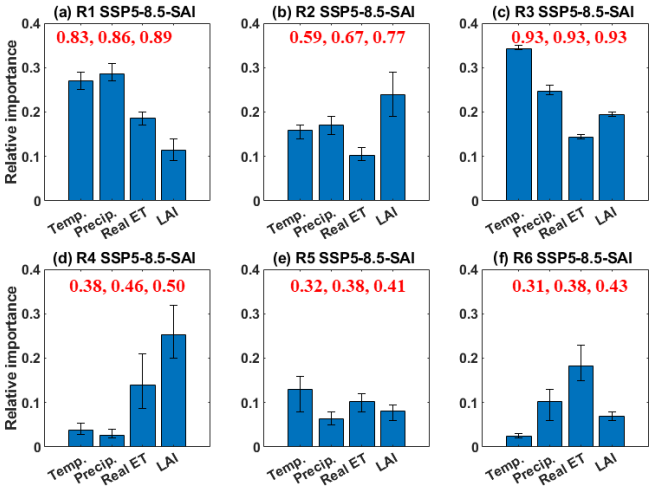

Figure 7. As in Fig. 6, but for the SSP5-8.5-SAI scenario.

play with other factors, such as vegetation coverage, temperature, and ET, plays a pivotal role. The vegetation coverage as the primary variable influencing changes in TWS in the MENA region substantially increases under global warming (Figs. S14 and S15). It has an important, but often complex and uncertain, role in surface water content (Lemordant et al., 2018; Trugman et al., 2018); the denser the vegetation coverage, the higher the evapotranspiration rates. Furthermore, although precipitation over a broad portion of MENA is lowered under SAI relative to global warming, the mean TWS, in general, increases across a broad portion of the MENA region in response to the intervention. TWS significantly increases over Iran and Iraq under SAI compared to historical and global warming (Fig. 4b) as gains in available water from decreased temperature and, in turn, ET are largely sufficient to compensate for decreased precipitation (Figs. S8 and S10), signifying that in addition to precipitation, the water storage also strongly depends on local temperature (Ajjur et al., 2021). As an example, around the Caspian Sea (R1), although the changes in precipitation imposed by global warming are simulated to have been fully restored by SAI, the temperature has not, and in turn, the TWS is not fully restored by SAI. This is consistent with MLR model results (Fig. 7a) in which, beyond the precipitation, temperature also plays an important role in TWS across R1. Other studies also found that changes in precipitation do not necessarily correlate with changes in surface water due to differences in precipitation and evaporation responses under SAI (Irvine et al., 2016).

Our findings, on the whole, suggest that the specific SAI scenario considered here could help water storage in the dry regions (R2, R4, R5, and R6), i.e., leads to higher soil moisture and TWS compared with both the historical conditions and pure GHG-induced global warming. Likewise, Dagon and Scharg (2017) documented a rise in mean water availability and soil moisture during the period of June to August in MENA using SolarGeo simulations, consistent with the significant reduction in daily maximum temperatures and ET across the Middle East. This works through the combined positive effects of (1) a substantial decrease in temperature and ET over the entire study area compared with SSP5-8.5 global warming and (2) the increased precipitation in the southern MENA dry regions relative to historical conditions. The Middle East may therefore benefit from the water enrichment from climate change through the implementation of solar intervention (Burnell, 2021). However, the wet and colder regions, particularly around the Mediterranean coasts, may have less water storage compared with the historical period but more water relative to the GHG scenario due to a significant decrease in ET under SAI. Simpson et al. (2019) also reported a noteworthy decline of 18.5 % in available water (precipitation minus evaporation) across the Mediterranean area under high GHG emissions, while it was partially reversed (only 5 %) by a decrease in evaporation under SAI.

Although SAI partially compensates for the extreme TWS changes in most of the study area, aligning with findings by Jones et al. (2018), the overall extreme TWS trend indicates an increase in dry regions of Iran and Iraq, the Arabian Peninsula, and western NA. Conversely, there is a substantial decrease in extreme TWS in the wetter lands around the Caspian and Mediterranean seas and, to lower degrees, in eastern NA compared to historical conditions. The implications of our findings under both future climate scenarios (SSP5-8.5 and SSP5-8.5-SAI) extend beyond hydrology and water resource management. Changes in TWS have significant implications for climate adaptation, flood and drought

risk management, and infrastructure planning. Some dry areas such as Iran, Iraq, and the Arabian Peninsula are projected to receive greater extreme TWS under both global warming and SAI or only SAI, and these regions have historically suffered from flooding (e.g., Abbaspour et al., 2009; Ghavidel and Jafari Hombari, 2020; Dezfuli et al., 2021). The significant increase in extreme TWS enhances their flood risks. Hence, governments in these regions should plan for adaptations to water megastructures such as dams on the large rivers of Karkheh and Karun in western Iran as well as the Euphrates and Tigris in Iraq, since they have been mostly designed with historical hydrology in mind.

There are several caveats and caution needed for our results. First, our findings are based on a single model simulation (CESM2) and a single scenario climate scenario, SSP5-8.5, with (three available realizations) and without (five available realizations) SAI. Future studies should consider alternative SAI scenarios to explore the sensitivity of our results to model and scenario choices. The SSP scenarios include some that clearly portray undesirable futures, especially the high-emissions SSP5 scenarios and the regional rivalry SSP3 that illustrate the danger of unchecked climate change (MacMartin et al., 2022). There are more caveats for the SAI experiment used here: (1) it deploys in 2020 and therefore does not simulate any plausible future, and (2) it takes into account solely the high-emissions scenario SSP5-8.5 that is suitable for capturing a high "signal" compared to internal variability. This is useful for understanding the science but inconsistent with present-day projections of mitigation attempts (Burgess et al., 2020). However, while the signal is stronger under high GHG emissions, it is plausible that the directions and patterns of response would be similar in a lower-emission experiment, with the magnitude of changes roughly depending on the degree of warming being suppressed by SAI (e.g., MacMartin et al., 2022).

5 Conclusions

The current study is the first attempt to understand the influence of GHG emissions and SAI scenarios on both mean and extreme water storage changes over the lands around the Caspian and Mediterranean seas, Middle East, and northern Africa under global warming and SAI scenarios compared to the historical 1985–2014 conditions. The mean TWS is projected to decrease across the wetter lands around the Caspian and Mediterranean seas to the north (3.7 %–5.2 % on average) but increase over most of the MENA region (up to 5.6 % over the Arabian Peninsula) that has a drier climate under high-GHG forcing compared to present-day conditions.

Although the SAI tends to reverse, to a degree, the significant changes in TWS revealed by SSP5-8.5 over the entire area, it significantly overcompensates for the slightly reduced TWS under the high-GHG scenario in Iran and Iraq. The MLR model analysis of driving factors suggests that the impacts of temperature on water storage changes, like precipitation, are also important under both high-GHG forcing and SAI scenarios. Although SAI mostly decreases precipitation over most of the domain, it is accompanied by higher mean TWS across the entire study area due to the cooler climate.

Although significant changes in extreme TWS under high GHG emissions are reduced by SAI, the changes due to future climate changes are still large relative to the historical period across a broad portion of the domain. With SAI, TWS significantly decreases in the eastern lands around the Caspian Sea while substantially increasing across the Middle East regions of Iran, Iraq, and the Arabian Peninsula. This may increase flood risks since water megastructures have been mostly designed with historical hydrology in mind. Finally, the SAI scenario appears to increase accessible water storage in the dry regions of the Middle East and northern Africa. The wetter and colder lands around the Caspian and Mediterranean Sea may have less available water compared with the historical conditions, although SAI partially ameliorates the changes imposed by global warming.

Data availability. The data for CESM2 simulations are publicly available via its website: https://esgf-node.llnl.gov/search/cmip6/ (last access: 1 October 2023, Earth System Grid Foundation, 2020). To access these specific data via the ESGF website use the source ID CESM2-WACCM, experiment ID ssp585, and frequency "mon". The SSP5-8.5-SAI data are freely available at https://www.earthsystemgrid.org/dataset/ucar.cgd.ccsm4.geomip.ssp5.html (https://doi.org/10.26024/t49k-1016) (last access: 2 October 2023, National Center for Atmospheric Research, 2020).

Supplement. The supplement related to this article is available online at: https://doi.org/10.5194/esd-15-91-2024-supplement.

Author contributions. AR coordinated the analysis, graphics of various figures, and paper preparation. KK and ST conceptualized and prepared the data. JCM conceptualized and coordinated the interpretation and discussion for various sections. All authors contributed to the discussion and writing.

Competing interests. The contact author has declared that none of the authors has any competing interests.

Disclaimer. Publisher's note: Copernicus Publications remains neutral with regard to jurisdictional claims made in the text, published maps, institutional affiliations, or any other geographical representation in this paper. While Copernicus Publications makes every effort to include appropriate place names, the final responsibility lies with the authors.

Special issue statement. This article is part of the special issue "Resolving uncertainties in solar geoengineering through multi-model and large-ensemble simulations (ACP/ESD inter-journal SI)". It is not associated with a conference.

Acknowledgements. We appreciate the financial support from the DEGREES Initiative in collaboration with the World Academy of Sciences (TWAS) under grant no. 4500443035.

Financial support. This research has been supported by the DEGREES Initiative in collaboration with the World Academy of Sciences (grant no. 4500443035).

Review statement. This paper was edited by Ben Kravitz and reviewed by two anonymous referees.

References

Abbaspour, K. C., Faramarzi, M., Ghasemi, S. S., and Yang, H.: Assessing the impact of climate change on water resources in Iran, Water Resour. Res., 45, W10434, https://doi.org/10.1029/2008WR007615, 2009.

Abdelmoaty, H. M., Papalexiou, S. M., Rajulapati, C. R., and AghaKouchak, A.: Biases beyond the mean in CMIP6 extreme precipitation: A global investigation, Earth's Future, 9, e2021EF002196, https://doi.org/10.1029/2021EF002196, 2021.

Abiodun, B. J., Odoulami, R. C., Sawadogo, W., Oloniyo, O. A., Abatan, A. A., New, M., Lennard, C., Izidine, P., Egbebiyi, T. S., and MacMartin, D. G.: Potential impacts of stratospheric aerosol injection on drought risk managements over major river basins in Africa, Clim. Change, 169, 1–19, https://doi.org/10.1007/s10584-021-03268-w, 2021.

Ajjur, S. B. and Al-Ghamdi, S. G.: Evapotranspiration and water availability response to climate change in the Middle East and North Africa, Clim. Change, 166, 28, https://doi.org/10.1007/s10584-021-03122-z, 2021.

Arjdal, K., Driouech, F., Vignon, E., Chéruy, F., Manzanas, R., Drobinski, P., Chehbouni, A., and Idelkadi, A.: Future of land surface water availability over the Mediterranean basin and North Africa: Analysis and synthesis from the CMIP6 exercise, Atmos. Sci. Lett., 24, e1180, https://doi.org/10.1002/asl.1180, 2023.

Arnell, N. W.: Climate change and global water resources, Glob. Environ. Change, 9, 31–49, https://doi.org/10.1016/S0959-3780(99)00017-5, 1999.

Babaousmail, H., Hou, R., Ayugi, B., Ojara, M., Ngoma, H., Karim, R., Rajasekar, A., and Ongoma, V.: Evaluation of the performance of CMIP6 models in reproducing rainfall patterns over North Africa, Atmosphere, 12, 475, https://doi.org/10.3390/atmos12040475, 2021.

Bağçaci, S. Ç., Yucel, I., Duzenli, E., and Yilmaz, M. T.: Intercomparison of the expected change in the temperature and the precipitation retrieved from CMIP6 and CMIP5 climate projections: A Mediterranean hot spot case, Turkey, Atmos. Res., 256, 105576, https://doi.org/10.1016/j.atmosres.2021.105576, 2021.

Bala, G., Duffy, P. B., and Taylor, K. E.: Impact of geoengineering schemes on the global hydrological cycle, P. Natl. Acad. Sci. USA, 105, 7664–7669, https://doi.org/10.1073/pnas.0711648105, 2008.

Bao, Y., Duan, L., Liu, T., Tong, X., Wang, G., Lei, H., Zhang, L., and Singh, V. P.: Simulation of evapotranspiration and its components for the mobile dune using an improved dual-source model in semi-arid regions, J. Hydrol., 592, 125796, https://doi.org/10.1016/j.jhydrol.2020.125796, 2021.

Barlow, M., Zaitchik, B., Paz, S., Black, E., Evans, J., and Hoell, A.: A review of drought in the Middle East and southwest Asia, J. Climate, 29, 8547–8574, https://doi.org/10.1175/JCLI-D-13-00692.1, 2016.

Bland, J. M. and Altman, D. G.: Multiple significance tests: the Bonferroni method, BMJ, 310, 170, https://doi.org/10.1136/bmj.310.6973.170, 1995.

Bucchignani, E., Mercogliano, P., Panitz, H. J., and Montesarchio, M.: Climate change projections for the Middle East–North Africa domain with COSMO-CLM at different spatial resolutions, Adv. Clim. Change Res., 9, 66–80, https://doi.org/10.1016/j. Accre.2018.01.004, 2018.

Burgess, M. G., Ritchie, J., Shapland, J., and Pielke, R.: IPCC baseline scenarios have over-projected CO_2 emissions and economic growth, Environ. Res. Lett., 16, 014016, https://doi.org/10.1088/1748-9326/abcdd2, 2020.

Burnell, L.: Risks to global water resources from geoengineering the climate with solar radiation management (Doctoral dissertation, University of Nottingham), PhD thesis, Item ID: 66269, 2021.

Cook, B. I., Smerdon, J. E., Seager, R., and Coats, S.: Global warming and 21st century drying, Clim. Dynam., 43, 2607–2627, https://doi.org/10.1007/s00382-014-2075-y, 2014.

Cook, B. I., Anchukaitis, K. J., Touchan, R., Meko, D. M., and Cook, E. R.: Spatiotemporal drought variability in the Mediterranean over the last 900 years, J. Geophys. Res.-Atmos., 121, 2060–2074, https://doi.org/10.1002/2015JD023929, 2016.

Cook, B. I., Mankin, J. S., Marvel, K., Williams, A. P., Smerdon, J. E., and Anchukaitis, K. J.: Twenty-first century drought projections in the CMIP6 forcing scenarios, Earth's Future, 8, e2019EF001461, https://doi.org/10.1029/2019EF001461, 2020.

Crook, J. A., Jackson, L. S., Osprey, S. M., and Forster, P. M.: A comparison of temperature and precipitation responses to different Earth radiation management geoengineering schemes, J. Geophys. Res.-Atmos., 120, 9352–9373, https://doi.org/10.1002/2015JD023269, 2015.

Cheng, W., MacMartin, D. G., Dagon, K., Kravitz, B., Tilmes, S., Richter, J. H., Mills, M. J., and Simpson, I. R.: Soil moisture and other hydrological changes in a stratospheric aerosol geoengineering large ensemble, J. Geophys. Res.-Atmos., 124, 12773–12793, https://doi.org/10.1029/2018JD030237, 2019.

Dai, A.: Increasing drought under global warming in observations and models, Nat. Clim. Change, 3, 52–58, https://doi.org/10.1038/nclimate1633, 2013.

Dagon, K. and Schrag, D. P.: Exploring the effects of solar radiation management on water cycling in a coupled land–atmosphere model, J. Climate, 29, 2635–2650, https://doi.org/10.1175/JCLI-D-15-0472.1, 2016.

Dagon, K. and Schrag, D. P.: Regional climate variability under model simulations of solar geoengineering, J. Geophys. Res.-

Atmos., 122, 12–106, https://doi.org/10.1002/2017JD027110, 2017.

Danabasoglu, G., Lamarque, J. F., Bacmeister, J., Bailey, D. A., DuVivier, A. K., Edwards, J., Emmons, L. K., Fasullo, J., Garcia, R., Gettelman, A., Hannay, C., Holland, M. M., Large, W. G., Lauritzen, P. H., Lawrence, D. M., Lenaerts, J. T. M., Lindsay, K., Lipscomb, W. H., Mills, M. J., Neale, R., Oleson, K. W., Otto-Bliesner, B., Phillips, A. S., Sacks, W., Tilmes, S., van Kampenhout, L., Vertenstein, M., Bertini, A., Dennis, J., Deser, C., Fischer, C., Fox-Kemper, B., Kay, J. E., Kinnison, D., Kushner, P. J., Larson, V. E., Long, M. C., Mickelson, S., Moore, J. K., Nienhouse, E., Polvani, L., Rasch, P. J., Strand, W. G., and Strand, W. G.: The community earth system model version 2 (CESM2), J. Adv. Model. Earth Sy., 12, e2019MS001916, https://doi.org/10.1029/2019MS001916, 2020.

Dezfuli, A., Bosilovich, M. G., and Barahona, D.: A dusty atmospheric river brings floods to the Middle East, Geophy. Res. Lett., 48, e2021GL095441, https://doi.org/10.1029/2021GL095441, 2021.

Doksum, K. A. and Sievers, G. L.: Plotting with confidence: Graphical comparisons of two populations, Biometrika, 63, 421–434, https://doi.org/10.2307/2335720, 1976.

Döll, P. and Flörke, M.: Global-Scale Estimation of Diffuse Groundwater Recharge; Institute of Physical Geography, Frankfurt University, Frankfurt am Main, Germany, https://www.uni-frankfurt.de/45217767/FHP_03_Doell_Floerke_2005.pdf (last access: 25 September 2023), 2005.

Döll, P., Trautmann, T., Gerten, D., Schmied, H. M., Ostberg, S., Saaed, F., and Schleussner, C. F.: Risks for the global freshwater system at 1.5 °C and 2 °C global warming, Environ. Res. Lett., 13, 044038, https://doi.org/10.1088/1748-9326/aab792, 2018.

Droogers, P., Immerzeel, W. W., Terink, W., Hoogeveen, J., Bierkens, M. F. P., van Beek, L. P. H., and Debele, B.: Water resources trends in Middle East and North Africa towards 2050, Hydrol. Earth Syst. Sci., 16, 3101–3114, https://doi.org/10.5194/hess-16-3101-2012, 2012.

Earth System Grid Foundation: United States Department of Energy, [data set], https://esgf-node.llnl.gov/search/cmip6/ (last access: 1 October 2023), 2020.

Evans, J. P. and Smith, R. B.: Water vapor transport and the production of precipitation in the eastern Fertile Crescent, J. Hydrometeorol., 7, 1295–1307, https://doi.org/10.1175/JHM550.1, 2006.

Eyring, V., Bony, S., Meehl, G. A., Senior, C. A., Stevens, B., Stouffer, R. J., and Taylor, K. E.: Overview of the Coupled Model Intercomparison Project Phase 6 (CMIP6) experimental design and organization, Geosci. Model Dev., 9, 1937–1958, https://doi.org/10.5194/gmd-9-1937-2016, 2016.

Fader, M., Shi, S., von Bloh, W., Bondeau, A., and Cramer, W.: Mediterranean irrigation under climate change: more efficient irrigation needed to compensate for increases in irrigation water requirements, Hydrol. Earth Syst. Sci., 20, 953–973, https://doi.org/10.5194/hess-20-953-2016, 2016.

Famiglietti, J. S.: The global groundwater crisis, Nat. Clim. Change, 4, 945–948, https://doi.org/10.1038/nclimate2425, 2014.

Faour, G., Mhawej, M., and Fayad, A.: Detecting changes in vegetation trends in the Middle East and North Africa (MENA) region using SPOT vegetation, Cybergeo, Europ. J. Geograph., 779, https://doi.org/10.4000/cybergeo.27620, 2016.

Fragaszy, S. R., Jedd, T., Wall, N., Knutson, C., Fraj, M. B., Bergaoui, K., Svoboda, M., Hayes, M., and McDonnell, R.: Drought Monitoring and Warning System for the Middle East and North Africa, B. Am. Meteorol. Soc., 101, 904–910, https://doi.org/10.1175/BAMS-D-18-0084.1, 2020.

Ghavidel, Y. and Jafari Hombari, F.: Synoptic analysis of unexampled super-heavy rainfall on April 1, 2019, in west of Iran, Nat. Hazards, 104 1567–1580, https://doi.org/10.1007/s11069-020-04232-0, 2020.

Gilleland, E.: Bootstrap methods for statistical inference, Part II: Extreme-value analysis, J. Atmos. Ocean. Tech., 37, 2135–2144, https://doi.org/10.1175/JTECH-D-20-0070.1, 2020.

Giorgi F.: Climate change hot-spots, Geophys. Res. Lett., 33, L08707, https://doi.org/10.1029/2006GL025734, 2006.

Giorgi, F. and Lionello, P.: Climate change projections for the Mediterranean region, Global Planet. Change, 63, 90–104, https://doi.org/10.1016/j.gloplacha.2007.09.005, 2008.

Govindasamy, B. and Caldeira, K.: Geoengineering Earth's radiation balance to mitigate CO_2-induced climate change, Geophys. Res. Lett., 27, 2141–2144, https://doi.org/10.1029/1999GL006086, 2000.

Grömping, U.: Relative importance for linear regression in R: the package relaimpo, J. Stat. Softw., 17, 1–27, https://doi.org/10.18637/jss.v017.i01, 2007.

Hobeichi, S., Abramowitz, G., Ukkola, A. M., De Kauwe, M., Pitman, A., Evans, J. P., and Beck, H.: Reconciling historical changes in the hydrological cycle over land, npj Clim. Atmos. Sci., 5, 17, https://doi.org/10.1038/s41612-022-00240-y, 2022.

Hofste, R. W., Reig, P., and Schleifer, L.: 17 countries, home to one-quarter of the world's population, face extremely high water stress, 2019.

Intergovernmental Panel on Climate Change (IPCC): Working Group I Contribution to the Sixth Assessment Report (AR6), Climate Change 2021: The Physical Science Basis, 2021, https://www.ipcc.ch/assessment-report/ar6/ (last access: 5 December 2022), 2021.

Irvine, P. J., Kravitz, B., Lawrence, M. G., and Muri, H.: An overview of the Earth system science of solar geoengineering, Wiley Interdiscip. Rev. Clim. Change, 7, 815–833, https://doi.org/10.1002/wcc.423, 2016.

Johnson, J. W. and LeBreton, J. M.: History and use of relative importance indices in organizational research, Organ. Res. Methods, 7, 238–257, https://doi.org/10.1177/1094428104266510, 2004.

Jones, A. C., Hawcroft, M. K., Haywood, J. M., Jones, A., Guo, X., and Moore, J. C.: Regional climate impacts of stabilizing global warming at 1.5 K using solar geoengineering, Earth's Future, 6, 230–251, https://doi.org/10.1002/2017EF000720, 2018.

Karami, K., Tilmes, S., Muri, H., and Mousavi, S. V.: Storm track changes in the Middle East and North Africa under stratospheric aerosol geoengineering, Geophys. Res. Lett., 47, e2020GL086954, https://doi.org/10.1029/2020GL086954, 2020.

Kim, D. W. and Byun, H. R.: Future pattern of Asian drought under global warming scenario, Theor. Appl. Climatol., 98, 137–150, https://doi.org/10.1016/j.ejrh.2022.101191, 2009.

Konapala, G., Mishra, A. K., Wada, Y., and Mann, M. E.: Climate change will affect global water availability through compounding changes in seasonal precipitation and evaporation, Nat.

Commun., 11, 3044, https://doi.org/10.1038/s41467-020-16757-w, 2020.

Kravitz, B., Rasch, P. J., Forster, P. M., Andrews, T., Cole, J. N., Irvine, P. J., Ji, D., Kristjánsson, J. E., Moore, J. C., Muri, H., and Niemeier, U.: An energetic perspective on hydrological cycle changes in the Geoengineering Model Intercomparison Project (GeoMIP), J. Geophys. Res.-Atmos., 118, 13087–13102, https://doi.org/10.1002/2013JD020502, 2013.

Lelieveld, J., Hadjinicolaou, P., Kostopoulou, E., Chenoweth, J., El Maayar, M., Giannakopoulos, C., Hannides, C., Lange, M. A., Tanarhte, M., Tyrlis, E., and Xoplaki, E.: Climate change and impacts in the Eastern Mediterranean and the Middle East, Clim. Change, 114, 667–687, https://doi.org/10.1016/j.envres.2022.114537, 2012.

Lemordant, L., Gentine, P., Swann, A. S., Cook, B. I., and Scheff, J.: Critical impact of vegetation physiology on the continental hydrologic cycle in response to increasing CO_2, P. Natl. Acad. Sci. USA, 115, 4093, https://doi.org/10.1073/pnas.1720712115, 2018.

Lian, X., Piao, S., Chen, A., Huntingford, C., Fu, B., Li, L. Z., Huang, J., Sheffield, J., Berg, A. M., Keenan, T. F., and McVicar, T. R.: Multifaceted characteristics of dryland aridity changes in a warming world, Nat. Rev. Earth Environ., 2, 232–250, https://doi.org/10.1038/s43017-021-00144-0, 2021.

Lindeman, R. H., Merenda, P. F., and Gold, R. Z.: Introduction to bivariate and multivariate analysis (No. 04, QA278, L553), Scott Foresman, Glenview, IL, Uniq ID: 5310754, 1980.

Lionello, P., Malanotte-Rizzoli, P., Boscolo, R., Alpert, P., Artale, V., Li, L., Luterbacher, J., May, W., Trigo, R., Tsimplis, M., and Ulbrich, U.: The Mediterranean climate: an overview of the main characteristics and issues, Environ. Earth Sci., 4, 1–26, https://doi.org/10.1016/S1571-9197(06)80003-0, 2006.

MacMartin, D. G., Visioni, D., Kravitz, B., Richter, J. H., Felgenhauer, T., Lee, W. R., Morrow, D. R., Parson, E. A., and Sugiyama, M.: Scenarios for modeling solar radiation modification, P. Natl. Acad. Sci. USA, 119, e2202230119, https://doi.org/10.1073/pnas.2202230119, 2022.

Mamalakis, A., Randerson, J. T., Yu, J. Y., Pritchard, M. S., Magnusdottir, G., Smyth, P., Levine, P. A., Yu, S., and Foufoula-Georgiou, E.: Zonally opposing shifts of the intertropical convergence zone in response to climate change, Nat. Clim. Change, 11, 143–151, https://doi.org/10.1038/s41558-020-00963-x, 2021.

Masson-Delmotte, V., Zhai, P., Pörtner, H.-O., Roberts, D., Skea, J., and Shukla, P. R.: Global Warming of 1.5 °C: IPCC Special Report on Impacts of Global Warming of 1.5 °C above Pre-industrial Levels in Context of Strengthening Response to Climate Change, Sustainable Development, and Efforts to Eradicate Poverty, Cambridge University Press, https://www.ipcc.ch/sr15/ (last access: 20 September 2023), 2022.

MedECC: Climate and Environmental Change in the Mediterranean Basin – Current Situation and Risks for the Future, in: First Mediterranean Assessment Report, edited by: Cramer, W., Guiot, J., Marini, K., Union for the Mediterranean, Plan Bleu, UNEP/MAP, Marseille, France, 632 pp., https://doi.org/10.5281/zenodo.4768833, 2020.

Milly, P. C., Dunne, K. A., and Vecchia, A. V.: Global pattern of trends in streamflow and water availability in a changing climate, Nature, 438, 347–350, https://doi.org/10.1038/nature04312, 2005.

Mooney, H., Cropper, A., and Reid, W.: Confronting the human dilemma, Nature, 434, 561–562, https://doi.org/10.1038/434561a, 2005.

Mousavi, S. V., Karami, K., Tilmes, S., Muri, H., Xia, L., and Rezaei, A.: Future dust concentration over the Middle East and North Africa region under global warming and stratospheric aerosol intervention scenarios, Atmos. Chem. Phys., 23, 10677–10695, https://doi.org/10.5194/acp-23-10677-2023, 2023.

Muthyala, R., Bala, G., and Nalam, A.: Regional scale analysis of climate extremes in an SRM geoengineering simulation, Part 1: precipitation extremes, Curr. Sci., 114, 1024–1035, 2018.

National Center for Atmospheric Research (NCAR): Climate Data Gateway at NCAR, [data set], https://www.earthsystemgrid.org/dataset/ucar.cgd.ccsm4.geomip.ssp5.html (last access: 2 October 2023), 2020.

Nooni, I. K., Ogou, F. K., Chaibou, A. A. S., Nakoty, F. M., Gnitou, G. T., and Lu, J.: Evaluating CMIP6 Historical Mean Precipitation over Africa and the Arabian Peninsula against Satellite-Based Observation, Atmosphere, 14, 607, https://doi.org/10.3390/atmos14030607, 2023.

Oroud, I. M.: The Impacts of Climate Change on Water Resources in Jordan, in: Climatic Changes and Water Resources in the Middle East and North Africa, edited by: Zereini, F., and Hötzl, H., Environ. Sci. Eng., Springer, Berlin, Heidelberg, https://doi.org/10.1007/978-3-540-85047-2_ 10, 2008.

Peel, M. C., Finlayson, B. L., and McMahon, T. A.: Updated world map of the Köppen-Geiger climate classification, Hydrol. Earth Syst. Sci., 11, 1633–1644, https://doi.org/10.5194/hess-11-1633-2007, 2007.

Pokhrel, Y., Felfelani, F., Satoh, Y., Boulange, J., Burek, P., Gädeke, A., Gerten, D., Gosling, S. N., Grillakis, M., Gudmundsson, L., and Hanasaki, N.: Global terrestrial water storage and drought severity under climate change, Nat. Clim. Change, 11, 226–233, https://doi.org/10.1038/s41558-020-00972-w, 2021.

Ricke, K. L., Morgan, M. G., and Allen, M. R.: Regional climate response to solar-radiation management, Nat. Geosci., 3, 537–541, https://doi.org/10.1038/ngeo915, 2010.

Ricke, K., Wan, J. S., Saenger, M., and Lutsko, N. J.: Hydrological Consequences of Solar Geoengineering, Annu. Rev. Earth Planet Sci., 51, 447–470, https://doi.org/10.1146/annurev-earth-031920-083456, 2023.

Reiter, L., Falk, H., Groat, C., and Coussens, C. M. (Eds): From Source Water to Drinking Water: Workshop Summary (National Academies Press, Washington DC, 2004), https://nap.nationalacademies.org/catalog/11142/from-source-water-to-drinking-water-workshop-summary (last access: 23 September 2023), 2004.

Robock, A., Oman, L., and Stenchikov, G. L.: Regional climate responses to geoengineering with tropical and Arctic SO_2 injections, J. Geophys. Res.-Atmos., 113, D16101, https://doi.org/10.1029/2008JD010050, 2008.

Sarle, W.: The VARCLUS Procedure, in: SAS/STAT User's Guide fourth, Vol. 2, 1641–1659, SAS Institute, Inc. http://support.sas.com/documentation/onlinedoc/stathttp://support.sas.com/documentation/onlinedoc/stat (last access: 2 October 2023), 1990.

Schewe, J., Heinke, J., Gerten, D., Haddeland, I., Arnell, N. W., Clark, D. B., Dankers, R., Eisner, S., Fekete, B. M., Colon-Gonzalez, F. J., Gosling, S. N., Kim, H., Liu, X., Masaki, Y.,

Portmann, F. T., Satoh, Y., Stacke, T., Tang, Q., Wada, Y., Wisser, D., Albrecht, T., Frieler, K., Piontek, F., Warszawski, L., and Kabat, P.: Multimodel assessment of water scarcity under climate change, P. Natl. Acad. Sci. USA, 111, 3245–3250, https://doi.org/10.1073/pnas.1222460110, 2014.

Shaban, A.: Impact of Climate Change on Water Resources of Lebanon: Indications of Hydrological Droughts, in: Climatic Changes and Water Resources in the Middle East and North Africa, edited by: Zereini, F. and Hötzl, H., Environ. Sci. Eng., Springer, Berlin, Heidelberg, https://doi.org/10.1007/978-3-540-85047-2_ 11, 2008.

Shiklomanov, I. A. and Rodda, J. C. (Eds): World Water Resources at the Beginning of the 21st Century (Cambridge Univ. Press, Cambridge, 2003), ISBN 9780521617222, 2003.

Simpson, I. R., Tilmes, S., Richter, J. H., Kravitz, B., MacMartin, D. G., Mills, M., Fasullo, J. J. T., and Pendergrass A. G.: The regional hydroclimate response to stratospheric sulfate geoengineering and the role of stratospheric heating, J. Geophys. Res.-Atmos., 124, 12587–12616, https://doi.org/10.1029/2019JD031093, 2019.

Scanlon, B. R., Fakhreddine, S., Rateb, A., de Graaf, I., Famiglietti, J., Gleeson, T., Grafton, R. Q., Jobbagy, E., Kebede, S., Kolusu, S. R., and Konikow, L. F.: Global water resources and the role of groundwater in a resilient water future, Nat. Rev. Earth Environ., 4, 87–101, https://doi.org/10.1038/s43017-022-00378-6, 2023.

Schleussner, C.-F., Lissner, T. K., Fischer, E. M., Wohland, J., Perrette, M., Golly, A., Rogelj, J., Childers, K., Schewe, J., Frieler, K., Mengel, M., Hare, W., and Schaeffer, M.: Differential climate impacts for policy-relevant limits to global warming: the case of 1.5 °C and 2 °C, Earth Syst. Dynam., 7, 327–351, https://doi.org/10.5194/esd-7-327-2016, 2016.

Suppan, P., Kunstmann, H., Heckl, A., Rimmer, A.: Impact of Climate Change on Water Availability, in: Climatic Changes and Water Resources in the Middle East and North Africa, edited by: Zereini, F., Hötzl, H., Environ. Sci. Eng., Springer, Berlin, Heidelberg, https://doi.org/10.1007/978-3-540-85047-2_ 5, 2008.

Tabari, H. and Willems, P.: Seasonally varying footprint of climate change on precipitation in the Middle East, Sci. Rep., 8, 4435, https://doi.org/10.1038/s41598-018-22795-8, 2018.

Tilmes, S., Fasullo, J., Lamarque, J. F., Marsh, D. R., Mills, M., Alterskjaer, K., Muri, H., Kristjánsson, J. E., Boucher, O., Schulz, M., and Cole, J. N.: The hydrological impact of geoengineering in the Geoengineering Model Intercomparison Project (GeoMIP), J. Geophys. Res.-Atmos., 118, 11–036, https://doi.org/10.1002/jgrd.50868, 2013.

Tilmes, S., Richter, J. H., Mills, M. J., Kravitz, B., MacMartin, D. G., Garcia, R. R., Kinnison, D. E., Lamarque, J. F., Tribbia, J., and Vitt, F.: Effects of different stratospheric SO_2 injection altitudes on stratospheric chemistry and dynamics, J. Geophys. Res.-Atmos., 123, 4654–4673, 2018.

Tilmes, S., MacMartin, D. G., Lenaerts, J. T. M., van Kampenhout, L., Muntjewerf, L., Xia, L., Harrison, C. S., Krumhardt, K. M., Mills, M. J., Kravitz, B., and Robock, A.: Reaching 1.5 and 2.0 °C global surface temperature targets using stratospheric aerosol geoengineering, Earth Syst. Dynam., 11, 579–601, https://doi.org/10.5194/esd-11-579-2020, 2020.

Trenberth, K. E.: Changes in precipitation with climate change, Clim. Res., 47, 123–138, https://doi.org/10.3354/cr00953, 2011.

Trugman, A. T., Medvigy, D., Mankin, J. S., and Anderegg, W. R. L.: Soil moisture stress as a major driver of carbon cycle uncertainty, Geophys. Res. Lett., 45, 6495–6503, https://doi.org/10.1029/2018GL078131, 2018.

Visioni, D., MacMartin, D. G., Kravitz, B., Boucher, O., Jones, A., Lurton, T., Martine, M., Mills, M. J., Nabat, P., Niemeier, U., Séférian, R., and Tilmes, S.: Identifying the sources of uncertainty in climate model simulations of solar radiation modification with the G6sulfur and G6solar Geoengineering Model Intercomparison Project (GeoMIP) simulations, Atmos. Chem. Phys., 21, 10039–10063, https://doi.org/10.5194/acp-21-10039-2021, 2021.

Waha, K., Krummenauer, L., Adams, S., Aich, V., Baarsch, F., Coumou, D., Fader, M., Hoff, H., Jobbins, G., Marcus, R., and Mengel, M.: Climate change impacts in the Middle East and northern Africa (MENA) region and their implications for vulnerable population groups, Reg. Environ. Change, 17, 1623–1638, https://doi.org/10.1007/s10113-017-1144-2, 2017.

Wang, J., Song, C., Reager, J. T., Yao, F., Famiglietti, J. S., Sheng, Y., MacDonald, G. M., Brun, F., Schmied, H. M., Marston, R. A., and Wada, Y.: Recent global decline in endorheic basin water storages, Nat. Geosci., 11, 926–932, https://doi.org/10.1038/s41561-018-0265-7, 2018.

Wang, Z., Zhan, C., Ning, L., and Guo, H.: Evaluation of global terrestrial evapotranspiration in CMIP6 models, Theor. Appl. Clim., 143, 521–531, https://doi.org/10.1007/s00704-020-03437-4, 2021.

World Bank: Beyond Scarcity: Water Security in the Middle East and North Africa. MENA Development Report, © Washington, DC: World Bank, http://hdl.handle.net/10986/27659 (last access: 6 Octobor 2023), License: CC BY 3.0 IGO, 2018.

Wu, W. Y., Lo, M. H., Wada, Y., Famiglietti, J. S., Reager, J. T., Yeh, P. J. F., Ducharne, A., and Yang, Z. L.: Divergent effects of climate change on future groundwater availability in key mid-latitude aquifers, Nat. Commun., 11, 3710, https://doi.org/10.1038/s41467-020-17581-y, 2020.

Wu, R. J., Lo, M. H., and Scanlon, B. R.: The annual cycle of terrestrial water storage anomalies in CMIP6 models evaluated against GRACE data, J. Climate, 34, 8205–8217, https://doi.org/10.1175/JCLI-D-21-0021.1, 2021.

United Nations Educational Scientific and Cultural Organization, UNESCO: Water for People – Water for Life, The United Nations World Water Development Report (Berghahn Books, Oxford, 2003), https://www.un.org/esa/sustdev/publications/WWDR_english_129556e.pdf (last access: 8 Octobor 2023), 2003.

Xiong, J., Guo, S., Abhishek, Chen, J., and Yin, J.: Global evaluation of the "dry gets drier, and wet gets wetter" paradigm from a terrestrial water storage change perspective, Hydrol. Earth Syst. Sci., 26, 6457–6476, https://doi.org/10.5194/hess-26-6457-2022, 2022.

Zamani, Y., Hashemi Monfared, S. A., Azhdari Moghaddam, M., and Hamidianpour, M.: A comparison of CMIP6 and CMIP5 projections for precipitation to observational data: the case of Northeastern Iran, Theor. Appl. Climatol., 142, 1613–1623, https://doi.org/10.1007/s00704-020-03406-x, 2020.

Zittis, G., Hadjinicolaou, P., Klangidou, M., Proestos, Y., and Lelieveld, J.: A multi-model, multi-scenario, and multi-domain analysis of regional climate projections for the

Mediterranean, Reg. Environ. Change, 19, 2621–2635, https://doi.org/10.1007/s10113-019-01565-w, 2019.

Zhang, B., Xia, Y., Long, B., Hobbins, M., Zhao, X., Hain, C., Li, Y., and Anderson, M. C.: Evaluation and comparison of multiple evapotranspiration data models over the contiguous United States: Implications for the next phase of NLDAS (NLDAS-Testbed) development, Agr. Forest Meteorol., 280, 107810, https://doi.org/10.1016/j.agrformet.2019.107810, 2020.

Zhang, X., Li, J., Wang, Z., and Dong, Q.: Global hydroclimatic drivers of terrestrial water storage changes in different climates, Catena, 219, 106598, https://doi.org/10.1016/j.catena.2022.106598, 2022.